WIND-TUNNEL INVESTIGATION OF VORTEX FLAPS ON A HIGHLY SWEPT INTERCEPTOR CONFIGURATION

W. Elliott Schoonover, Jr.
Aeronautical Engineer
NASA Langley Research Center
Hampton, Virginia USA

and

Willard E. Ohlson
Specialist Engineer
Boeing Military Airplane Company
Seattle, Washington USA

Abstract

A subsonic wind-tunnel investigation of the application of vortex flaps to a supersonic interceptor configuration is described. Experimental results are presented which indicate the aerodynamic effects of vortex-flap deflection, trailing-edge flap deflection, vortex flap chord and span, vertical stabilizers, and a highly cambered leading edge designed for attached flow. Data presented include longitudinal forces and moments, upper-surface pressure distributions, and oil- and smoke-flow visualization photographs. It is concluded that a full-span deployable vortex flap can provide a substantial performance improvement for this and other similar configurations.

Symbols

$\bar{c}$	mean aerodynamic chord
C_D	drag coefficient $\left(\frac{D}{q_\infty S_{ref}}\right)$
C_L	lift coefficient $\left(\frac{L}{q_\infty S_{ref}}\right)$
C_m	pitching moment coefficient $\left(\frac{M}{q_\infty S_{ref} \bar{c}}\right)$
C_{p_u}	upper surface pressure coefficient $\left(\frac{p_{s_u} - p_\infty}{q_\infty}\right)$
c_r	wing root chord
D	drag force
L	lift force
M	pitching moment (positive nose up)
M_∞	freestream Mach number
p_{s_u}	upper surface static pressure
p_o	freestream total pressure
p_∞	freestream static pressure
q_∞	freestream dynamic pressure
R_1, R_2	primary and secondary reattachment
$Re_{\bar{c}}$	freestream Reynolds number based on $\bar{c}$
S_{ref}	wing reference area
S_1, S_2	primary and secondary separation
V_∞	freestream velocity
x	longitudinal coordinate in body-axis system, measured from leading edge of wing root chord (inches, positive aft)
α	model angle of attack (deg)
γ	ratio of specific heats for air
δ_{BF}	body flap deflection (deg, positive trailing edge down)
δ_{EV}	elevon deflection (deg, positive trailing edge down)
δ_{VF}	vortex flap deflection (deg, positive leading edge down)
ν_∞	freestream kinematic viscosity

Introduction

Aircraft wings that are highly swept for efficiency at supersonic cruising speeds develop leading-edge separation and upper surface vortex flow at higher angles of attack (e.g., takeoff/landing and maneuvering). These vortices create substantial increases in the lifting force generated by the wing, but at the expense of increased drag, due to the loss of leading-edge suction caused by the separation. The Polhamus suction analogy[1] demonstrates the relationship between the loss in leading-edge suction and the gain in lift for sharp leading edges. More recent studies explore the influences on this relationship of rounded leading edges[2] and Reynolds number[3]. For flight conditions requiring high lift, this trade of leading-edge thrust for increased lift is beneficial; however, for maneuvers requiring the maximum available engine thrust, minimizing drag by maintaining attached flow, and thus leading-edge

thrust, can be desirable. Unfortunately, experience has shown that maintaining attached leading-edge flow at high sweep angles can be extremely difficult, or impossible. Lamar, et al, found, in the course of an investigation[4] aimed at optimizing a cambered leading-edge vortex design, that high levels of leading-edge thrust could be obtained with stabilized leading-edge vortices acting on a suitably cambered leading edge and that this thrust effect could be approximated by a simple deflected leading-edge surface. The "vortex flap" concept, described in reference 5, evolved from this finding.

The vortex flap, illustrated in figure 1, is a hinged leading-edge control surface, suitably sized and deflected to generate a vortex whose reattachment line lies on, or near, the hinge. This not only recovers part of the thrust loss due to the leading-edge separation by having the low-pressure region beneath the vortex act upon a forward facing surface, but also promotes flow attachment over the remainder of the wing.

Recent studies [6-10], explore the performance potential and design optimization for vortex flaps applied to basic wing planforms. Research is also underway to evaluate the application of vortex flaps to both current and future aircraft configurations. This paper presents results from a wind-tunnel test of vortex flaps applied to an advanced supersonic interceptor configuration.

Wind-Tunnel Model and Test Conditions

This investigation was conducted in the NASA Langley Research Center 7- by 10-Foot High-Speed Tunnel. The tests were conducted at $M_\infty = 0.3$ ($Re_{\bar{c}} = 6.6 \times 10^6$) with a few checks for Mach number effects at $M_\infty = 0.6$ ($Re_{\bar{c}} = 10.5 \times 10^6$). Balance load limits restricted the model angle of attack to about 24^o at $M_\infty = 0.3$ and 12^o at $M_\infty = 0.6$.

The baseline model, a supersonic interceptor designed for efficient cruise at Mach 3.0[11], is shown installed in the wind tunnel in figure 2(a). The wing leading edge (cruise design) detaches and is replaceable with a leading edge designed to maintain attached flow at typical maneuvering angles of attack. The vertical stabilizers, nacelles, and outboard wingtips also detach. The elevons and body flap can be set at various deflection combinations of 0^o, 5^o, 10^o, and 20^o. The model has 85 static pressure ports, arranged on both upper and lower surfaces in six spanwise rows, as shown in figure 2(b).

The vortex flaps used in this investigation, shown in figure 2(c), were designed using as a guide the findings of Rao[12] regarding vortex flaps applied to a 74^o delta wing. The flaps are secured to the wing leading edge by mounting brackets set to various deflection angles and any inter-surface gaps are filled with body fill. The inboard portions of these flaps are instrumented with 16 static pressure ports arranged in two rows which line up with the third and fifth rows of wing pressure ports. Also shown in figure 2(c), are the baseline planform and the attached flow leading edge. The cross-section sketch of the attached flow design points out its large camber and sharp leading edge. All pressures were measured by a precision scanivalve system contained within the model fuselage. Forces and moments were measured by a six-component strain gauge balance also contained within the model fuselage. Following completion of the force and pressure testing, oil-flow and smoke-flow photographs were taken to aid in the interpretation of features noted in the force and pressure data.

Results and Discussion

This paper presents the influences of vortex flap deflection, trailing-edge flap deflection, vortex flap chord and span, the vertical stabilizers, and the highly cambered attached-flow leading edge. Force and moment coefficients are presented in the stability axis system and are referenced to the basic wing planform area, under the assumption of a deployable leading edge. The effects of added wing area are presented separately.

Vortex Flap Deflection

Because the intent is to form and confine the leading-edge vortex to the vortex flap surface itself, and because vortices grow and move inboard with increasing angle of attack, it was thought that the deflection of the vortex flap would have a pronounced effect upon its performance. A drag polar showing the effects of vortex flap deflections of 30^o, $30^o/45^o$ (twisted flap), and 45^o at zero trailing-edge flap deflection is presented in figure 3. Also shown are theoretical boundaries derived by applying a vortex-lattice code[13] to the baseline model's planform (no camber included). The lower drag boundary defines the lift-drag relationship corresponding to full leading-edge suction (i.e., attached flow). The higher drag boundary corresponds to zero leading-edge suction (i.e., fully separated flow) plus the accompanying vortex lift. Both boundaries include a zero-lift drag correction of $C_{D_o} = .012$. A line is drawn spanning these boundaries at a lift coefficient of 0.5, which is typical of maneuvering flight for slender wing configurations. The horizontal scale above defines the percentage of suction achieved for $C_L = .5$ at various levels of drag.

Figure 3 shows that, beginning at relatively low levels of lift, the drag of the cruise configuration tends toward the zero suction/vortex flow boundary as the lift increases and the leading-edge vortices become the dominant influence on the wing pressures, and, thus, its loading. At $C_L = 0.5$, only about 7 percent of the theoretically available leading-edge suction is obtained. Adding the basic vortex flap shown in figure 2(c) results in a substantial increase in the suction obtained and a corresponding reduction in drag. The amount of flap deflection, however, had little influence.

The pressure distributions corresponding to this set of drag polars and a lift coefficient of approximately 0.5 are shown in figure 4. Here the upper surface pressures are shown plotted normal to and measured from the wing and flap upper surfaces, so that the thrusting effect of moving the vortex onto the flap becomes apparent. The lower surface pressures are not shown because they

consistently show only a typical attached-flow variation with angle of attack. In figure 4, it is apparent that the vortex flap has indeed moved the leading-edge vortex outboard onto a more forward facing surface. In fact, over the forward half of the wing the vortex reattachment line appears to have been kept on, or very near, the flap hinge line. Over the aft half of the wing, the vortex moves progressively from a position above the flap inboard over the hinge line and onto the wing surface itself. Note, however, that at $\frac{x}{c_r} = 0.478$ and $\frac{x}{c_r} = 0.877$ the spanwise displacement of the vortex is about equal to the increase in the wing semispan and that, even at the most aft station, some leading-edge thrust has been recovered. Figure 4 also shows that the various vortex-flap deflections had little effect on the vortex position, although, as one would expect, the higher flap deflections and resulting reductions in leading-edge angle of attack did produce weaker vortices and thus lower suction levels. This contrasts with data obtained by Rao at lower deflection angles for a constant chord vortex flap on a 74° delta wing (presented by Frink in ref. 10). In that study, increasing flap deflection ($\delta_{VF} = 0^o$, 10^o, 20^o) resulted in higher levels of suction beneath the vortex. The suction increase between $\delta_{VF} = 10^o$ and $\delta_{VF} = 20^o$, however, was less than that between $\delta_{VF} = 0^o$ and $\delta_{VF} = 10^o$, suggesting a possible decrease in suction levels at higher deflection angles.

Drag polars for the baseline configuration and various vortex flap deflections with the trailing edge flaps deflected to 20° are shown in figure 5. Here again, at $C_L \approx 0.5$, a substantial drag improvement above that provided by the trailing-edge deflection is evident, although the increment is smaller than that obtained with no trailing-edge flap deflection (fig. 3). The influence of vortex flap deflection is again small. The best flap deflection tested was the smallest, $\delta_{VF} = 30^o$. Figure 6 presents these same results in terms of lift-to-drag ratio versus lift coefficient. The full-suction and zero-suction boundaries shown on this and subsequent similar figures are those predicted for the baseline supersonic camber configuration and $\delta_{BF} = \delta_{EV} = 0^o$ by the vortex-lattice method and include the zero-lift drag correction. At lift coefficients above 0.35, the vortex flaps produce an increase in performance. At a lift coefficient $C_L = 0.5$, the vortex flaps increase the realized L/D increment due to leading-edge thrust recovery from 26 percent to as much as 44 percent of that theoretically possible.

These performance results are similar to those obtained by Marchman[6] for vortex flaps applied to a 75° swept delta wing. In that case, compared to the L/D increment obtained by adding a vortex flap, the difference in performance between a 30° vortex flap deflection and a 40° deflection was small, and for $C_L \approx 0.5$, the 40° deflection appeared to be optimal.

Because most of the vortex flap surface area lies forward of the baseline configurations aerodynamic center, the flap has a destabilizing effect, as demonstrated by the pitching moment data in figure 7. This effect is consistent with that of added forward area in attached flow. The higher vortex flap deflections appear to both moderate somewhat and delay to higher lift levels the pitchup due to leading-edge vortex formation.

Trailing-Edge Flap Deflection

The influence of trailing-edge flap deflection on the drag polar of the basic 45° vortex flap is shown in figure 8. The filled symbols correspond to a constant angle of attack of about 13°, and show that, for a constant vortex flap deflection, increasing trailing-edge flap deflection results in greater lift, greater drag, and a net increase in performance. At $C_L = 0.5$, equal and increasing deflection of both the body flap (δ_{BF}) and elevon (δ_{EV}) consistently increased the level of leading-edge thrust recovered. Note, however, that for $\delta_{BF} = 20^o$, the amount of elevon deflection (10° or 20°) had little effect on performance, although $\delta_{EV} = 20^o$ did provide some performance improvement at higher lift levels.

Upper surface pressure distributions for the various trailing-edge flap deflections and $\alpha \approx 13^o$ are shown in figure 9 and indicate that the influence of trailing-edge deflection is confined to the aft quarter of the wing root chord. Over that portion of the vortex flap, increasing trailing edge deflection appears to have had no effect on the size or spanwise location of the leading-edge vortex. It did, however, result in somewhat increased levels of suction beneath the vortex, which in turn contributed to the improved performance. It is conjectured that the increased suction beneath the vortex is due to an increase in vortex strength, which, in turn, is brought about by the increased circulation (caused by trailing-edge deflection) and the consequently higher leading-edge upwash.

The effects of trailing-edge flap deflections on pitching moment are presented in figure 10 and show that the trailing-edge flaps remain effective in generating pitching moment for trim at lift coefficients greater than those required for maneuver. The destabilizing effect of the vortex flap is not influenced and the pitchup due to leading-edge vortex formation occurs in all vortex flap cases at $\alpha \approx 9.4^o$, though the corresponding lift coefficient is, or course, higher with increased trailing-edge deflection.

In summary, the trailing-edge flap was found to have little influence on the force and moment effects of the leading-edge vortex. These results are in agreement with those obtained by Marchman and Grantz for trailing-edge flaps deflected on a 75° delta wing with vortex flaps[7].

Vortex Flap Chord and Span

In an attempt to increase the extent of vortex flap traversed by the vortex core, various extensions of the vortex flap chord and span were

tested. The resulting drag polars are shown in figure 11, and the corresponding pressures in figure 12. The pressure data (fig. 12) are for a higher angle of attack (~17.5°) and lift coefficient (~.75) than those shown previously, because the effects of flap geometry on the pressures are more easily seen. Increasing the chord of the basic vortex flap (fig. 2(c)) did result in some drag improvement by moving the vortex outward onto a more forward-facing surface. This effect is evident in the pressures along the entire length of the flap, but its major influence on drag occurs at the aft end. As before, the outboard displacement of the vortex core appears to be roughly equivalent to the increase in semispan.

A much more substantial drag reduction at maneuver-typical lift coefficients was obtained by extending the wide-chord vortex flap to full span (fig. 2(c)). At the lift coefficient $C_L = 0.5$, the fraction of leading-edge suction recovered increased to 80 percent (fig. 11). Pressure data, shown in figure 12, indicate a slight increase in strength and outboard displacement of the vortex at the aft row of orifices, but not enough to account for much of the drag effect apparent in figure 11. To help understand these effects, oil-flow photographs of the extended chord, full-span configuration are shown in figure 13. Three distinct vortices are apparent. The largest is shed from the inboard portion of the vortex flap and rolls up, first completely over the vortex flap and then, toward the trailing edge, over the wing's upper surface. The attachment line for this vortex appears to cross the hinge line from the vortex flap onto the wing upper surface between $\frac{x}{c_r} = 0.478$ and $\frac{x}{c_r} = 0.583$, in agreement with the pressure data. A second, much smaller vortex, is shed from the hinge line of the outer vortex flap beginning at the break in hinge-line sweep (which also coincides approximately with the vertical stabilizer apex), and rolls up over the outboard wingtip. A third vortex forms over the outboard vortex flap, beginning at the junction with the inboard vortex flap. This vortex and the attached flow behind it, acting on the outboard vortex flap, with its reduced sweep angle, provides a substantial amount of thrust recovery. Figure 14 presents the influences of vortex flap chord and span in terms of L/D vs C_L. Employing the wide chord vortex flap over the full span increased the L/D improvement due to thrust recovery from 26 percent to 69 percent at the lift coefficient $C_L = 0.5$.

A further benefit of adding the outboard vortex flap surface is evident in the pitching moment characteristics, shown in figure 15. The destabilizing effect of adding the basic vortex flap to the baseline configuration is increased slightly, as one would expect, by the increase in vortex flap chord. Addition to the vortex flap span, because it falls behind the configuration's aerodynamic center, has a stabilizing effect, giving the configuration a small static margin. Thus, it appears that a careful selection of vortex flap chord and deflection applied over the full span of the configuration could provide a substantial improvement in trimmed flight performance.

Vertical Stabilizers

Flow visualization (fig. 13) indicated that, at lift levels typical of maneuver, the primary leading-edge vortex traversed the aft portion of the wing inboard of the vertical stabilizer, with another, smaller vortex forming on the wingtip outboard of the vertical stabilizer. This was true for the baseline configuration and both part-span and full-span vortex flaps, and suggested that some lift improvement might be obtained by removing the vertical stabilizers, thereby encouraging the main vortex to spread outboard over more of the span on the aft wing. Figure 16 shows the drag effects of removing the vertical stabilizers from the wide-chord, full-span, vortex-flap configuration. For $C_L < 0.8$, both lift and drag were reduced, for a slight performance improvement. However, for $C_L > 0.8$ (not shown), both the lift and the drag increased. The corresponding effects on pitching moment are shown in figure 17 and indicate that without the stabilizer a nose-down deviation develops between $C_L \approx 0.6$ ($\alpha \approx 14°$) and $C_L \approx 0.9$ ($\alpha \approx 19°$). This deviation does not occur with the stabilizer in place. For $C_L < 0.8$ ($\alpha \approx 17.5°$), removing the stabilizer caused a nose-up pitching-moment increment; however, for $C_L > 0.8$, removal caused a nose-down pitching moment increment. Upper-surface pressure distributions at the aft two orifice stations are shown in figure 18 for $\alpha = 12.9°$ and $\alpha = 17.7°$. These data indicate that the nose-down pitching moment deviation between $C_L \approx 0.6$ and $C_L \approx 0.9$ occurs as the leading-edge vortex on the aft part of the wing moves from the vortex-flap surface onto the wing upper surface. They also show that even at the aft orifice row, which is just ahead of the vertical stabilizer apex, the pressure distribution is affected very little, so that the nose-down pitching moment deviation is due primarily to flow changes aft of that station.

Oil-flow visualization of the surface streamlines, shown in figure 19, suggest an explanation of these flow changes. Marked on the photographs are the approximate locations of the primary vortex reattachment line and secondary separation line (see inset sketch). At $\alpha = 12.9°$ (left side of figure), the main vortex reattachment line lies near the flap hinge line; i.e., the vortex is located over the flap. The vortex turns upward and streamwise at the sweep break, crossing the outboard vortex flap hinge just outboard of the stabilizer, and trails downstream between the outboard surface of the stabilizer and the upper surface of the wingtip. This suggests that removing the stabilizer allows the vortex to shift upward, away from the wingtip, thereby reducing the lift and causing a nose-up pitching moment increment. At $\alpha \approx 16.5°$ (right side of figure 19), the main vortex trails downstream inboard of the vertical stabilizer. The substantial upward flow visible on the inboard surface of the stabilizer is caused by impingement of the vortex. This suggests that, for $C_L > 0.8$, removing the stabilizer allows the vortex to move downward, closer to the wingtip, thereby increasing the lift and causing a nose-down pitching moment increment. The vertical stabilizer thus appears to moderate

the lift, drag, and pitching moment transients caused by the inboard movement of the vortex with increasing angle of attack. Further research will be required to determine the effects of the inboard sweep of the vortex on the lateral-directional stability and control.

Attached Flow Leading Edge

An attached flow, highly cambered, leading edge (see fig. 2c) was designed using leading-edge upwash data from an attached flow panel code[14]. The intent was to maintain attached flow over the cambered leading edge and onto the wing surface up to a maneuver angle of attack of 10^{o}. The drag polar for this configuration with a trailing-edge flap defleciton of 20^{o} is shown in figure 20. Also shown for comparison are data for the supersonic leading edge and the wide-chord, full-span, vortex flap. At all angles of attack, the attached flow leading edge produced lower lift and lower drag than the baseline (supersonic) leading edge, but the two drag polars are practically identical. For $C_L < 0.5$, the drag at constant lift is slightly higher for the cambered leading edge. For $C_L > 0.5$, the drag is slightly lower for the cambered leading edge. The divergence in the two polars at the right edge of the figure ($C_D \approx 0.14$) coincides with a momentary nose-down excursion in the pitching moment data, which is presented in figure 21. Upper-surface pressure distributions for the attached-flow leading edge configuration are compared in figure 22 with those for the supersonic leading edge and the wide-chord, full-span, vortex flap at $C_L \approx 0.5$ and $C_L \approx 0.7$, which bracket this drag and pitching moment anomaly. The pressure data indicate that the anomaly is caused by the formation of a vortex on the aft portion of the wing over this range of lift coefficient. The pressure data also indicate that at $C_L \approx 0.5$ the attached-flow leading edge ($\alpha \approx 12.5^{o}$) does, indeed, maintain attached flow over the upper surface, with the possible exception of a minor pressure peak at the aft station at about 60 percent of the semispan. Oil-flow and smoke-flow tracings of the upper-surface flow patterns at $\alpha \approx 6^{o}$, 8^{o}, and 12^{o}, which are presented in figure 23, support this interpretation. At $\alpha \approx 6^{o}$ ($C_L \approx 0.3$), the oil flow and smoke flow both indicate fully-attached flow. The inboard edge of the bright smoke region appears to coincide with the spanwise point ($\sim 70\%$) along $\frac{x}{c_r} = 0.723$ at which the spanwise component of the local surface-flow velocity changes sign. At $\alpha \approx 8^{o}$ ($C_L \approx 0.4$), both oil and smoke flows indicate that the flow over the cambered leading edge is attached. The flow, however, does separate just inboard of the "knee" of the upper surface (line S_1 in the figure) and reattaches at R_1, forming a weak vortex that is responsible for the minor pressure peak noted in figure 22. This vortex is similar to one observed in reference 15, wherein tailored leading-edge droop was used to maintain attached flow on the upper surface of a configuration quite similar to the present model. That vortex was attributed to a fairly sharp corner introduced near the wingtip by the rather high leading-edge deflection. As the angle of attack increases, the primary separation S_1 moves outboard over the cambered leading edge. At $\alpha \approx 12^{o}$, S_1 has reached the leading edge and the main vortex, which is now closer to the leading edge, begins to gain in strength as α increases, creating the much stronger pressure peak evident in figure 22 at $C_L \approx 0.7$. Initially, this stronger vortex forms over the aft portion of the wing, producing the nose-down pitching moment divergence evident at $C_L \approx 0.6$. However, small increases in angle of attack move the more forward portions of the primary separation line (S_1) progressively outboard so that by $C_L \approx 0.7$ the entire leading edge is separated, and the normal pitchup with increasing angle of attack (and resultant vortex strength) takes over. A secondary separation (S_2) and reattachment (R_2) are also visible in the oil flows (fig. 23) at $\alpha \approx 12^{o}$.

It is noteworthy that, although the cambered leading edge functioned as intended by maintaining attached flow onto the upper surface to an angle of attack greater than 12^{o}, its performance, as indicated by the drag polar, is essentially the same as that of the supersonic leading edge. This is because the influence of the additional leading-edge thrust recovered at any given angle of attack was nullified by the higher angle of attack necessary to obtain a given amount of lift. This finding emphasizes the performance advantage provided by the deployable vortex flap.

Planform Area Correction

The substantial performance improvement provided by the wide-chord, full-span, vortex flap (fig. 20), as compared to the supersonic leading edge and the attached flow leading edge, is, in fact, due to both a greater aerodynamic efficiency and an increase in planform area. The latter factor allowed maintaining constant lift at a constant angle of attack while simultaneously recovering leading-edge thrust, and is integral to the concept of a deployable vortex flap. However, to indicate how much of the performance improvement is attributable to aerodynamics, L/D vs C_L for the three configurations is presented in figure 24, with and without correction for planform area changes. Without the area correction (fig. 24(a)), adding the vortex flap to the cruise configuration (with $\delta_{BF} = \delta_{EV} = 20^{o}$) increases the L/D at $C_L = 0.5$ from 5.0 to 6.5. This L/D increase of 1.5 is equivalent to an increase from 26 percent to 69 percent in the fraction of the zero-suction to full-suction L/D increment that is obtained. With the area correction (fig. 24(b)), the corresponding L/D increase is from 5.0 to 5.6 which is equivalent to an increase from 26 percent to 45 percent in the fraction of the zero-suction to full-suction L/D increment that is obtained. As noted before, this purely aerodynamic effect is due primarily to the relatively unswept outer panel of the vortex flap.

Conclusions

For this and other similar configurations, properly sized and deflected vortex flaps, in combination with suitable trailing edge deflections, provide a flexible and powerful aerodynamic tool for improving vehicle performance in maneuvering flight.

At lift levels typical of maneuvering flight, the addition of a vortex flap provides significant improvement in the level of leading-edge suction by shifting the leading-edge vortex outboard onto a forward-facing surface. Combined vortex flap deflection and trailing-edge flap deflection provides better performance than deflection of either surface alone.

The level of leading-edge suction obtained with the basic vortex flap shows only a slight sensitivity to vortex flap deflection angle. The sensitivity is somewhat increased by trailing-edge flap deflection.

The deflection angle of the basic vortex flap has no apparent effect on the longitudinal instability caused by the vortex flap, but higher deflections do moderate the pitchup which occurs as the vortex moves from the vortex flap onto the wing.

Increased trailing-edge flap deflection improves the performance of the basic vortex flap. That improvement is due to strengthening (as opposed to growth or displacement) of the leading-edge vortex acting on the vortex flap.

Trailing-edge flap deflection has no apparent effects on stability and generated moments adequate for trim throughout the lift range tested. Trim effects are consistent with those typical of attached flow.

Some performance improvement is obtained by increasing the chord of the basic vortex flap. A much larger improvement (allowing 80-percent leading-edge suction recovery) is obtained by extending the wide-chord vortex flap full span. This substantial effect is due to the combination of a small separate vortex and attached flow, acting on the relatively unswept vortex-flap outer panel. Extending the vortex flap full span also restores longitudinal static stability to the configuration.

The vertical stabilizers moderate the lift, drag, and pitching moment deviations due to vortex growth and movement from the vortex flap onto the wing with increasing angle of attack. However, additional research is required to determine the effects of the vertical stabilizers on lateral-directional stability and control.

The leading edge designed for attached flow at an angle of attack $\alpha = 10^{o}$ does maintain attached flow on the wing upper surface to an angle of attack between 6^{o} and 7^{o}, where separation just inboard of the leading-edge "knee" results in a weak vortex. Leading-edge separation and the resulting strong upper-surface vortex flow is delayed to an angle of attack of about 12^{o}. Performance of the attached-flow leading edge, however, is equivalent to that of the baseline (supersonic) leading edge, apparently because the influence of the additional leading-edge suction obtained at a given angle of attack is effectively nullified by the higher angle of attack necessary to maintain a given amount of lift.

Applying the wide-chord, full-span, vortex flap to the cruise configuration with $\delta_{BF} = \delta_{EV} = 20^{o}$, provides an aerodynamic improvement in L/D of 0.6 at $C_L = 0.5$. This L/D increment is equivalent to an increase from 26 percent to 45 percent in the fraction of the the zero-suction to full-suction L/D increment that is obtained.

References

[1]Polhamus, Edward C.: A concept of the Vortex Lift of Sharp-Edge Delta Wings Based on a Leading-Edge Suction Analogy. NASA TN D-3767, 1966.

[2]Kulfan, R. M.: Wing Geometry Effects on Leading-Edge Vortices. AIAA Paper No. 79-1872, August, 1979.

[3]Carlson, Harry W.; Mack, Robert J.; and Barger, Raymond L.: Estimation of Attainable Leading-Edge Thrust for Wings at Subsonic and Supersonic Speeds. NASA TP-1500, October 1979.

[4]Lamar, J. E.; Schemensky, R. T.; and Reddy, C. S.: Development of a Vortex-Lift Design Procedure and Application to a Slender Maneuver-Wing Configuration. Journal of Aircraft, Vol. 18, No. 4, pp. 259-266, April 1981.

[5]Rao, D. M.: Leading-Edge "Vortex Flaps" for Enhanced Subsonic Aerodynamics of Slender Wings. ICAS Paper No. 80-13.5, October 1980.

[6]Marchman, J. F., III: Effectiveness of Leading-Edge Vortex Flaps on 60 and 75 Degree Delta Wings. Journal of Aircraft, Vol. 18, No. 4, pp. 280-286, April 1981.

[7]Marchman, J. F., III; and Grantz, A. C.: Trailing-Edge Flap Influence on Leading-Edge Vortex Flap Aerodynamics. AIAA Paper No. 82-0128, January 1982.

[8]Luckring, J. M.; Schoonover, W. E., Jr.; and Frink, N. T.: Recent Advances in Applying Free Vortex Sheet Theory for the Estimation of Vortex Flow Aerodynamics. AIAA Paper No. 82-0095, January 1982.

[9]Rao, D. M.: Upper Vortex Flap - A Versatile Surface for Highly-Swept Wings. ICAS Paper No. 82-6.7.1, August 1982.

[10]Frink, N. T.: Analytical Study of Vortex Flaps on Highly Swept Delta Wings. ICAS Paper No. 82-6.7.2, August 1982.

[11]Shrout, Barrett L.; and Fournier, Roger H.: Aerodynamic Characteristics of a Supersonic Cruise Airplane Configuration at Mach Numbers of 2.30, 2.96, and 3.30. NASA TM-78792, January 1979.

[12]Rao, D. M.: Leading-Edge Vortex Flap Experiments on a 74 Deg. Delta Wing. NASA CR-159161, November 1979.

[13]Lamar, John E.; and Gloss, Blair B.: Subsonic Aerodynamic Characteristics of Interacting Lifting Surfaces with Separated Flow Around Sharp Edges Predicted by a Vortex-Lattice Method. NASA TN D-7921, September 1975.

[14]Woodward, F. A.; Tinoco, E. N.; and Larsen, J. W.: Analysis and Design of Supersonic Wing-Body Combinations, Including Flow Properties in the Near Field, Part I - Theory and Applications. NASA CR-73106, 1967.

[15]Coe, Paul L., Jr.; Huffman, Jarrett K.; and Fenbert, James W.: Leading-Edge Deflection Optimization for a Highly Swept Arrow-Wing Configuration. NASA TP-1777, December 1980.

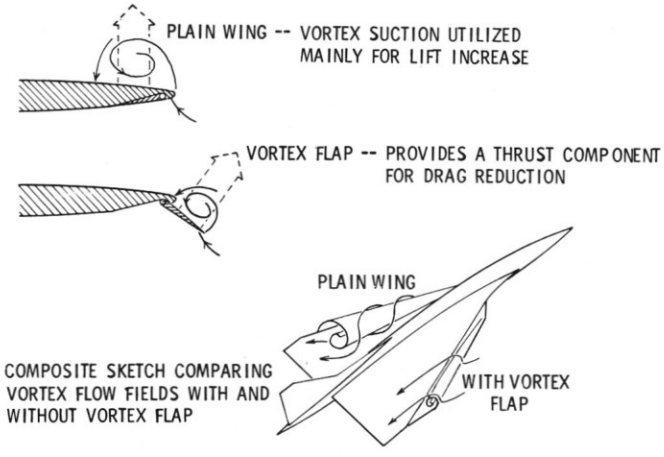

Figure 1. The Vortex Flap Concept.

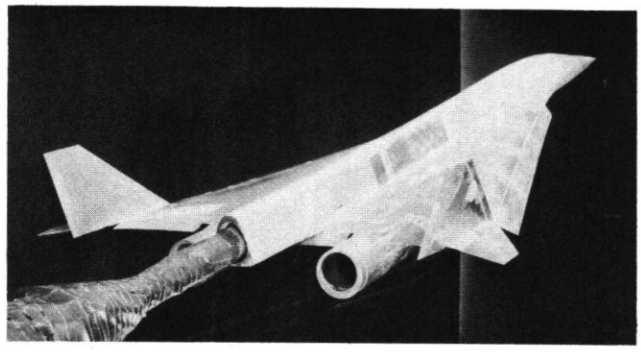

(a) Installation in Langley 7- by 10-Foot High-Speed Wind Tunnel

Figure 2. Supersonic Interceptor Wind Tunnel Model with Vortex Flaps.

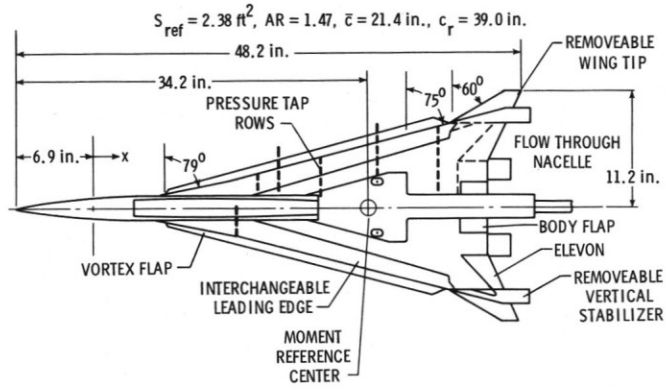

(b) Components and Dimensions

Figure 2. continued.

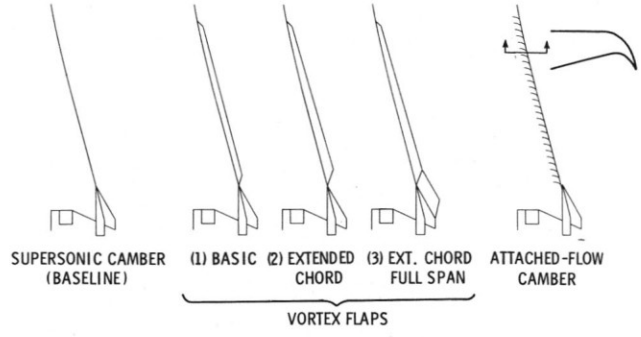

(c) Leading Edges

Figure 2. Concluded.

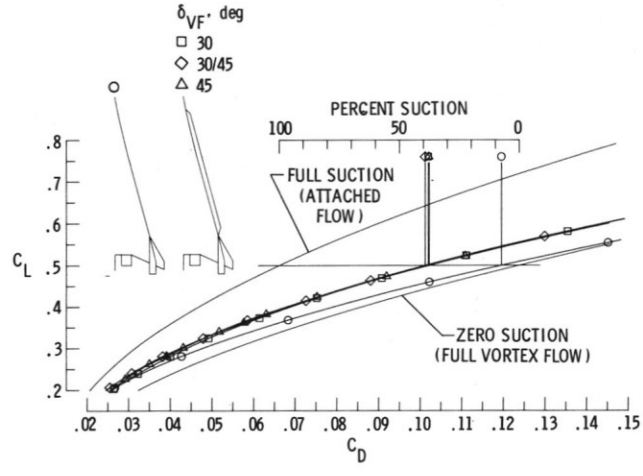

Figure 3. Vortex Flap Deflection Effects--Drag Polar. $M_\infty = 0.3$, $\delta_{BF} = \delta_{EV} = 0^o$.

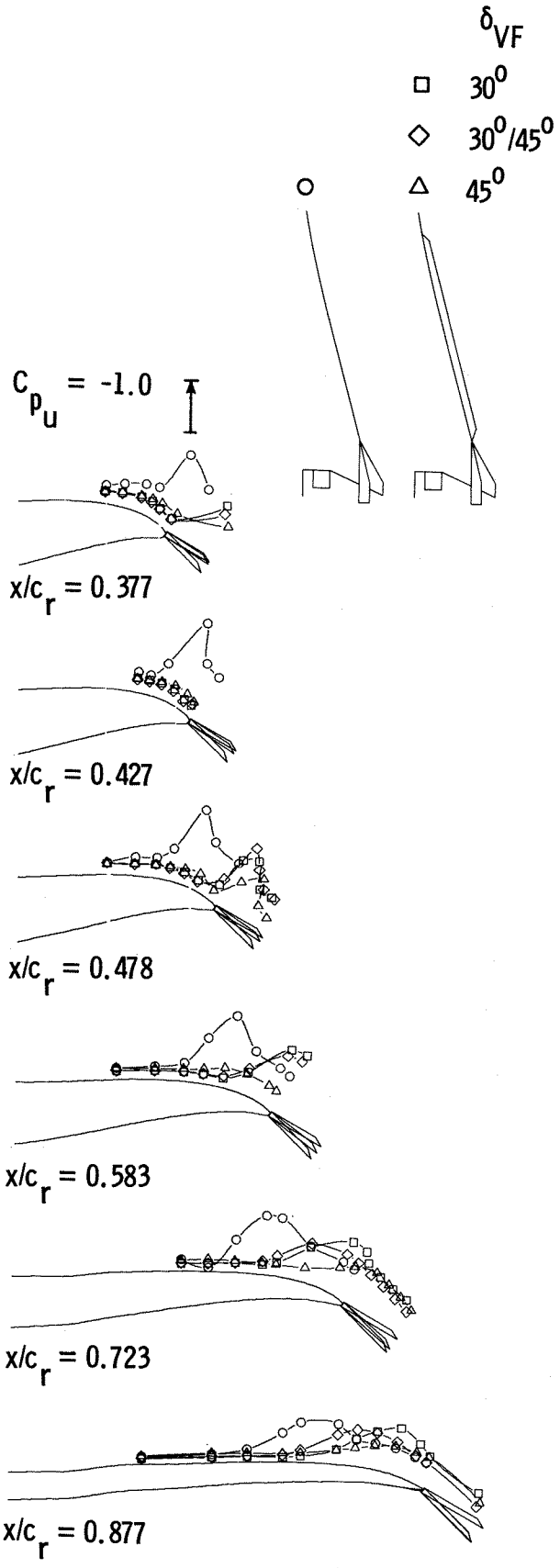

Figure 4. Vortex Flap Deflection Effects--Upper Surface Pressures. $M_\infty = 0.3$, $\alpha \approx 13^o$, $\delta_{BF} = \delta_{EV} = 0^o$.

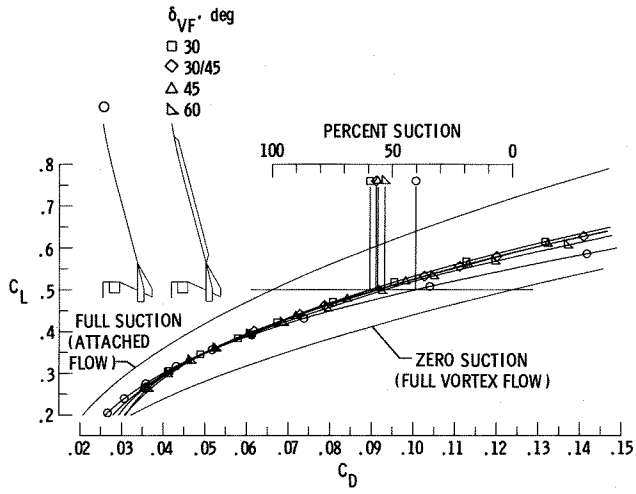

Figure 5. Vortex Flap Deflection Effects--Drag Polar. $M_\infty = 0.3$, $\delta_{BF} = \delta_{EV} = 20^o$.

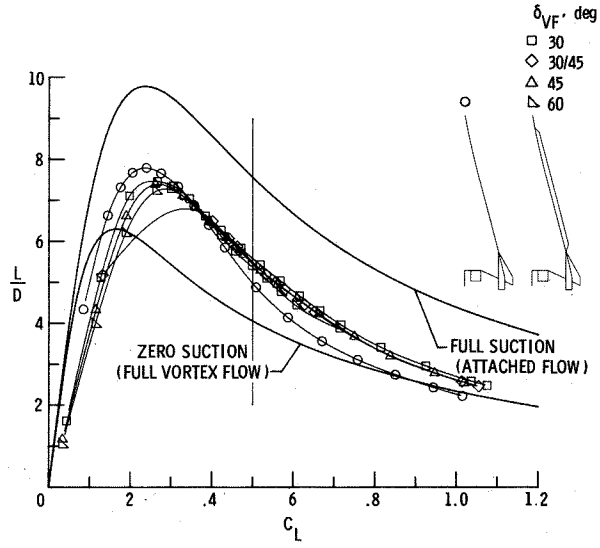

Figure 6. Vortex Flap Deflection Effects--Lift/Drag Ratio. $M_\infty = 0.3$, $\delta_{BF} = \delta_{EV} = 20^o$.

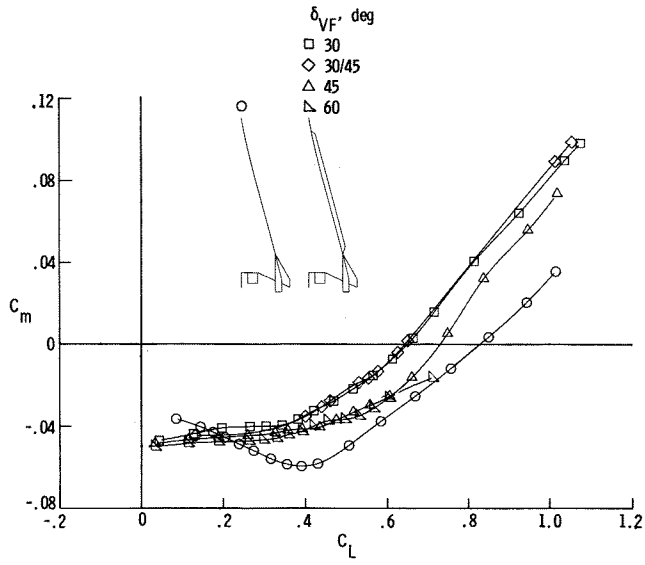

Figure 7. Vortex Flap Deflection Effects--Pitching Moment. $M_\infty = 0.3$, $\delta_{BF} = \delta_{EV} = 20^o$.

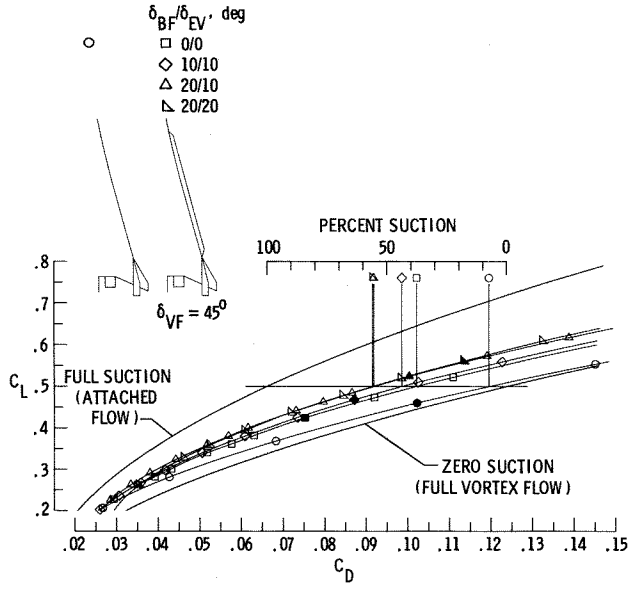

Figure 8. Body-Flap/Elevon Deflection Effects--Drag Polar. $M_\infty = 0.3$.

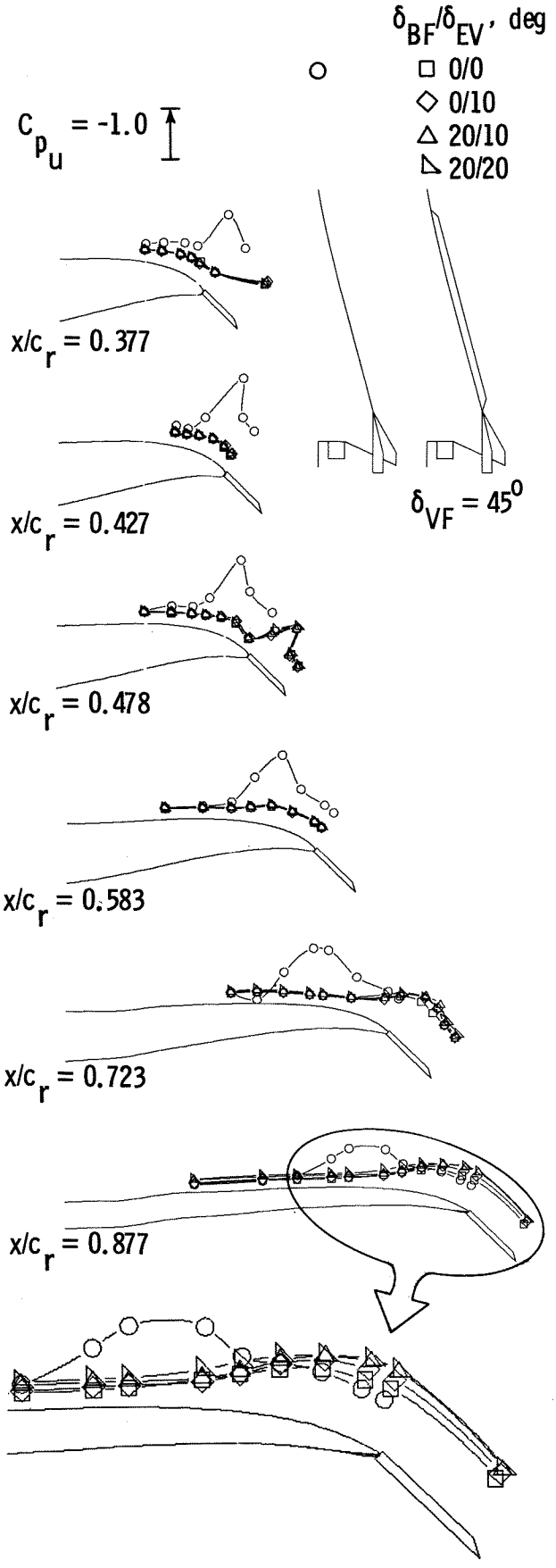

Figure 9. Body-Flap/Elevon Deflection Effects--Upper Surface Pressures. $M_\infty = 0.3$, $\alpha \approx 13^o$.

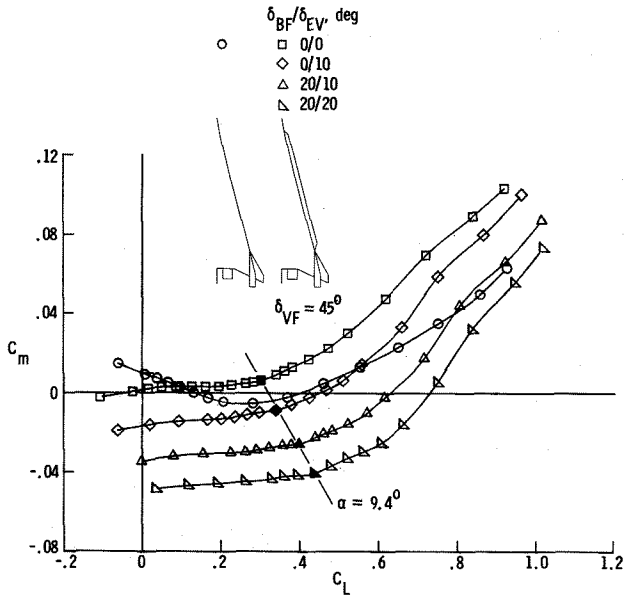

Figure 10. Body-Flap/Elevon Deflection Effects--Pitching Moment. $M_\infty = 0.3$.

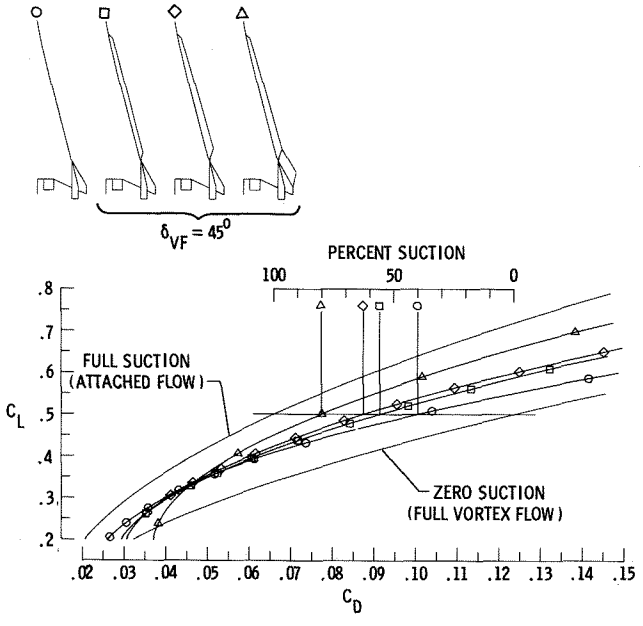

Figure 11. Vortex Flap Planform Effects--Drag Polar. $M_\infty = 0.3$, $\delta_{BF} = \delta_{EV} = 20^o$.

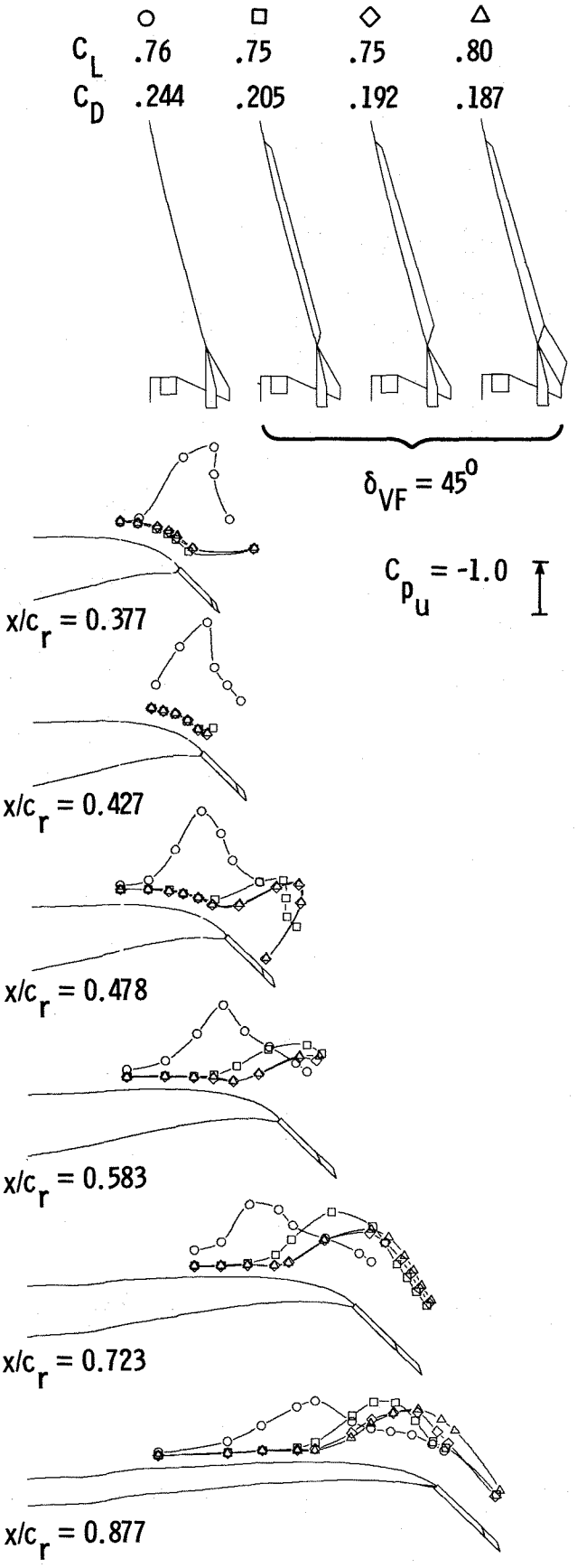

Figure 12. Vortex Flap Planform Effects--Upper Surface Pressures. $M_\infty = 0.3$, $\alpha \approx 18^o$, $\delta_{BF} = \delta_{EV} = 20^o$.

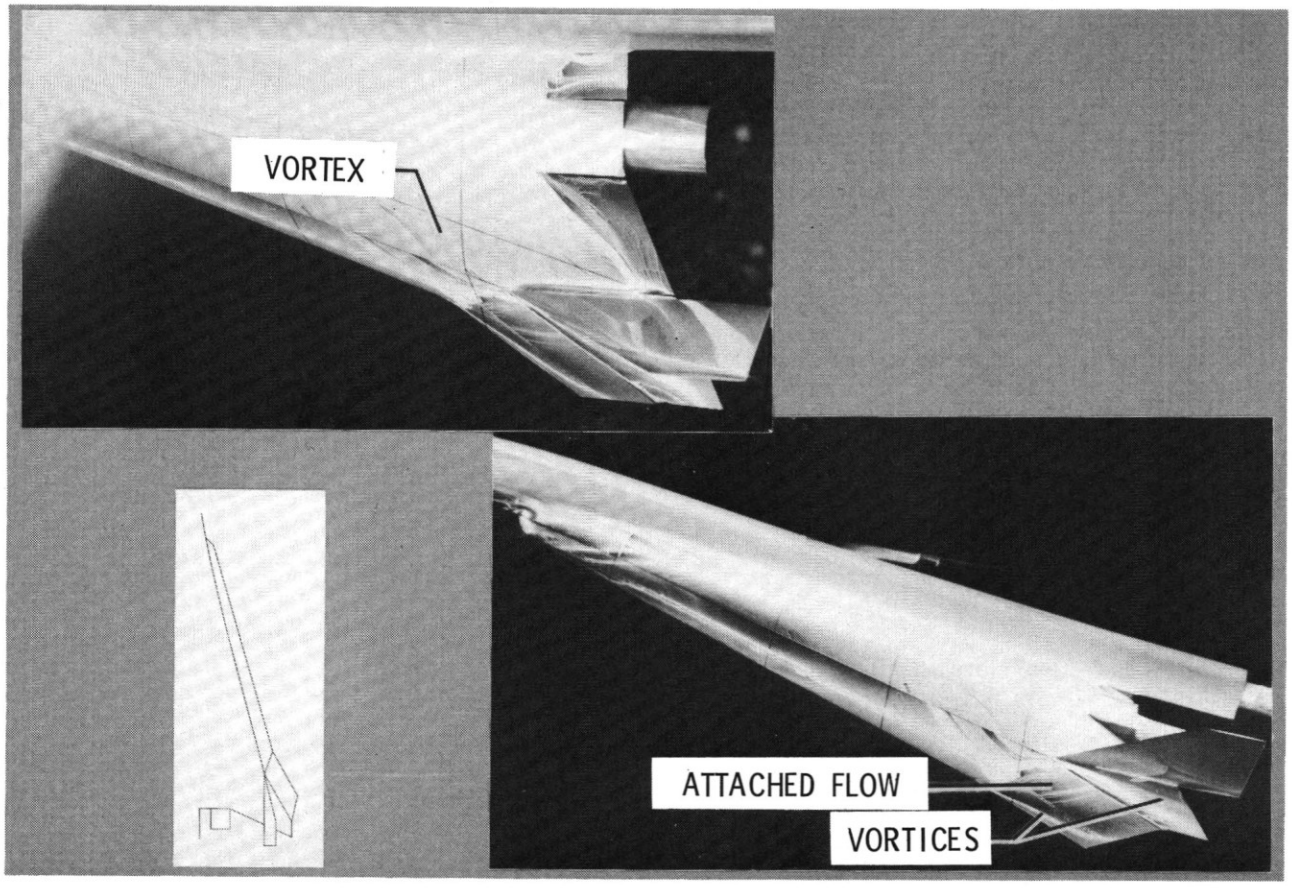

Figure 13. Wide Chord, Full-Span Vortex Flap Upper Surface Streamlines. $M_\infty = 0.3$, $\alpha \approx 16.5$, $\delta_{VF} = 45^o$, $\delta_{BF} = \delta_{EV} = 20^o$.

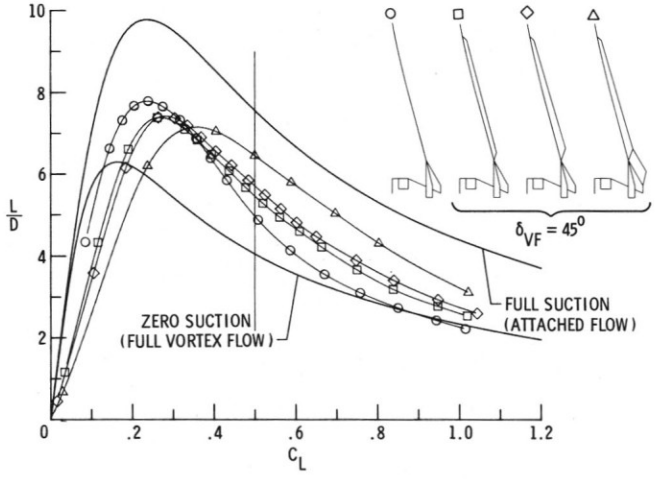

Figure 14. Vortex Flap Planform Effects--Lift/Drag Ratio. $M_\infty = 0.3$, $\delta_{BF} = \delta_{EV} = 20^o$.

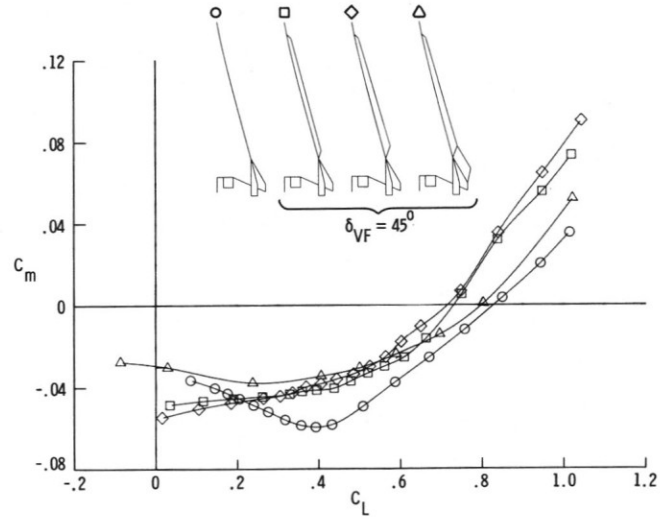

Figure 15. Vortex Flap Planform Effects--Pitching Moment. $M_\infty = 0.3$, $\delta_{BF} = \delta_{EV} = 20^o$.

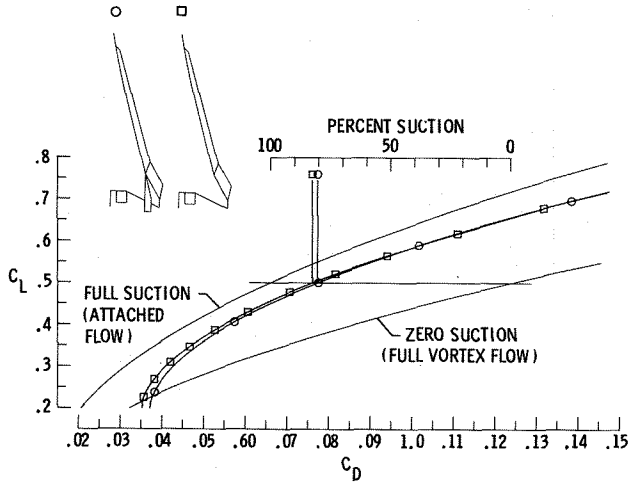

Figure 16. Vertical Stabilizer Effects--Drag Polar. $M_\infty = 0.3$, $\delta_{VF} = 45^0$, $\delta_{BF} = \delta_{EV} = 20^0$.

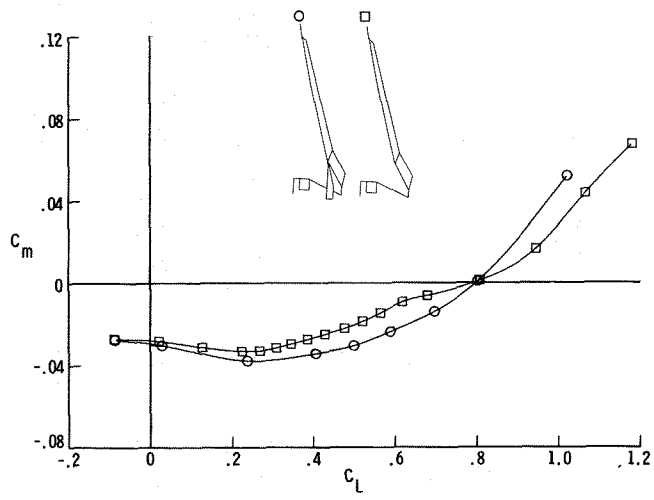

Figure 17. Vertical Stabilizer Effects--Pitching Moment. $M_\infty = 0.3$, $\delta_{VF} = 45^0$, $\delta_{BF} = \delta_{EV} = 20^0$.

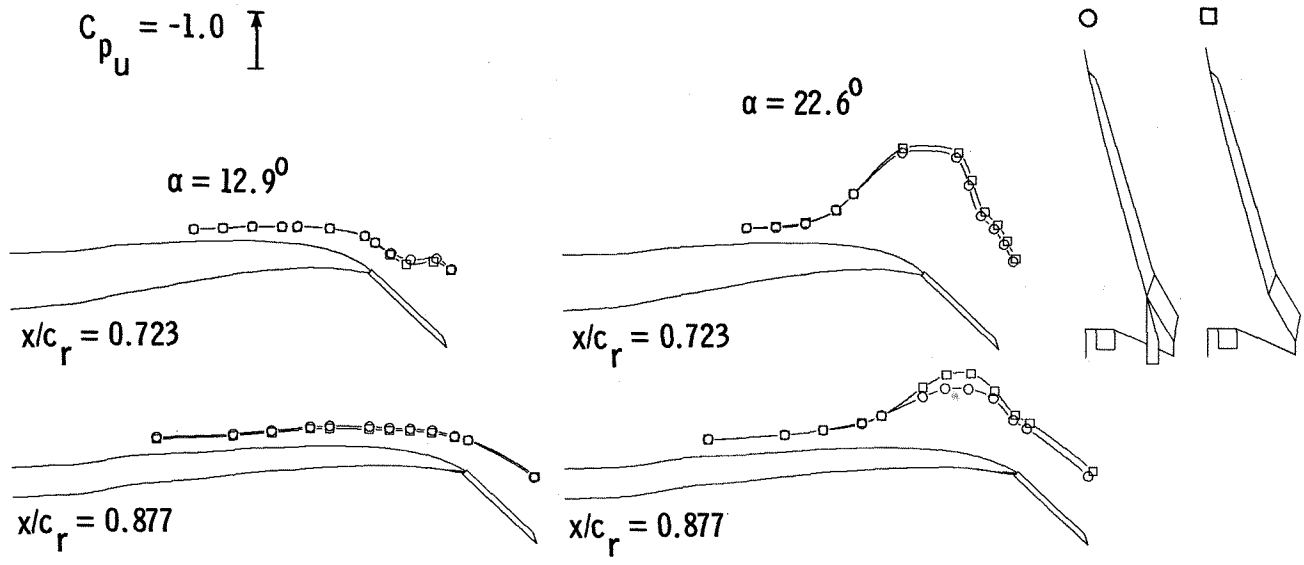

Figure 18. Vertical Stabilizer Effects--Upper Surface Pressures. $M_\infty = 0.3$, $\delta_{VF} = 45^0$, $\delta_{BF} = \delta_{EV} = 20^0$.

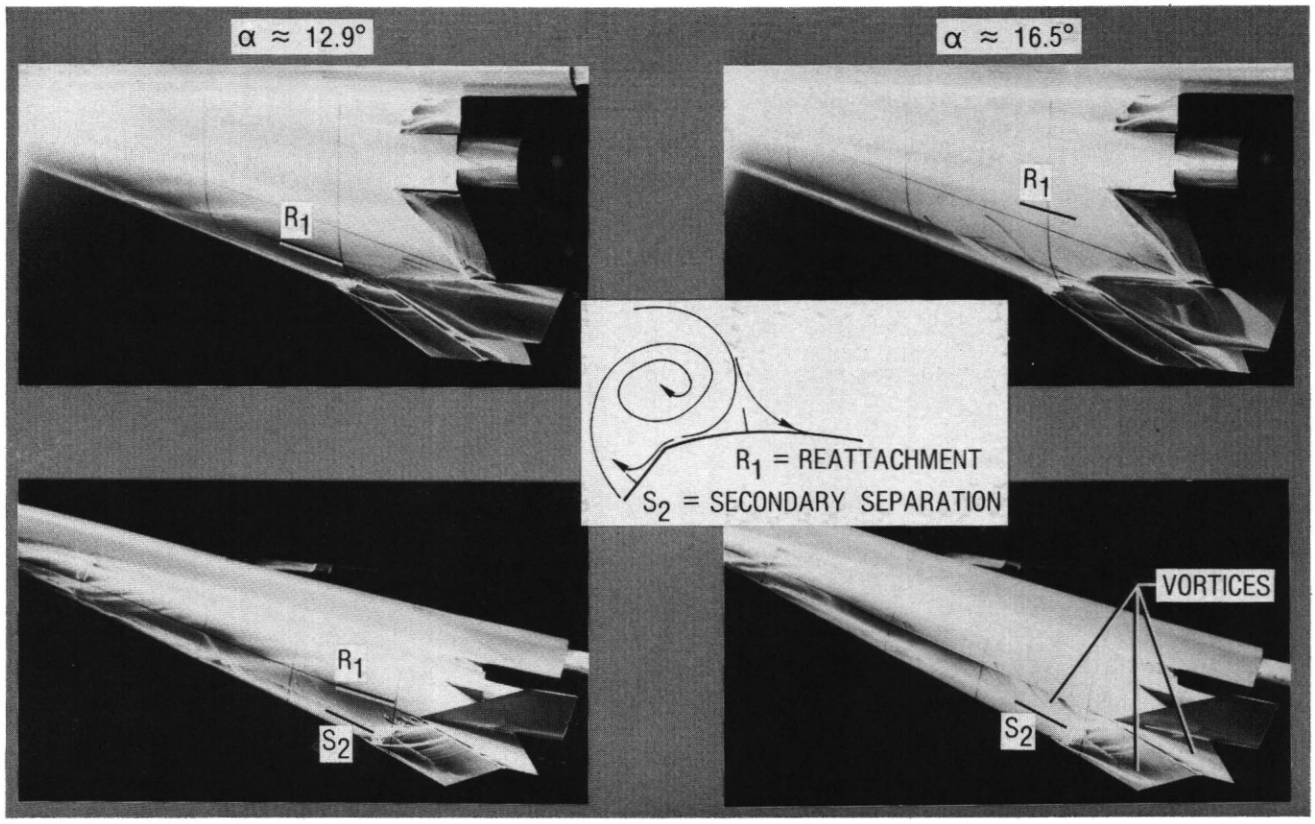

Figure 19. Wing, Vortex Flap, and Vertical Stabilizer Surface Streamlines. $M_\infty = 0.3$, $\delta_{VF} = 45^o$, $\delta_{BF} = \delta_{EV} = 20^o$.

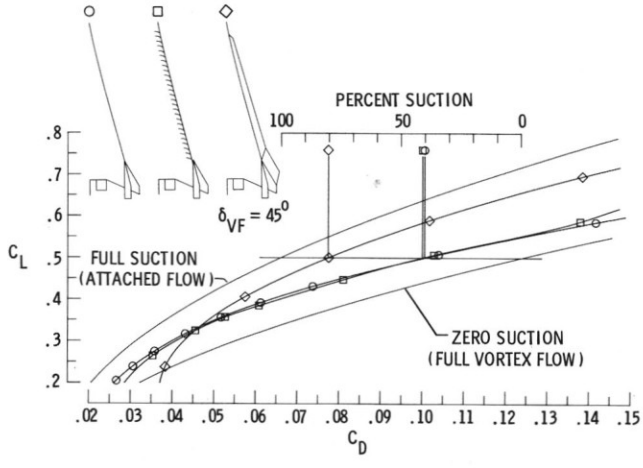

Figure 20. Cambered Leading-Edge/Vortex Flap Comparison--Drag Polar. $M_\infty = 0.3$, $\delta_{BF} = \delta_{EV} = 20^o$.

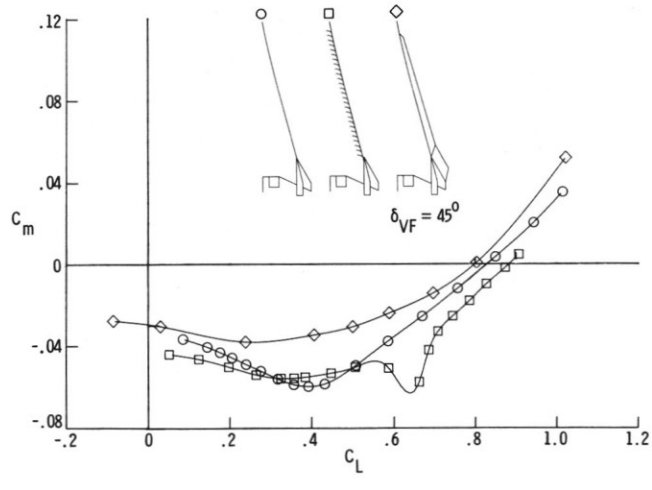

Figure 21. Cambered Leading-Edge/Vortex-Flap Comparison--Pitching Moment. $M_\infty = 0.3$, $\delta_{BF} = \delta_{EV} = 20^o$.

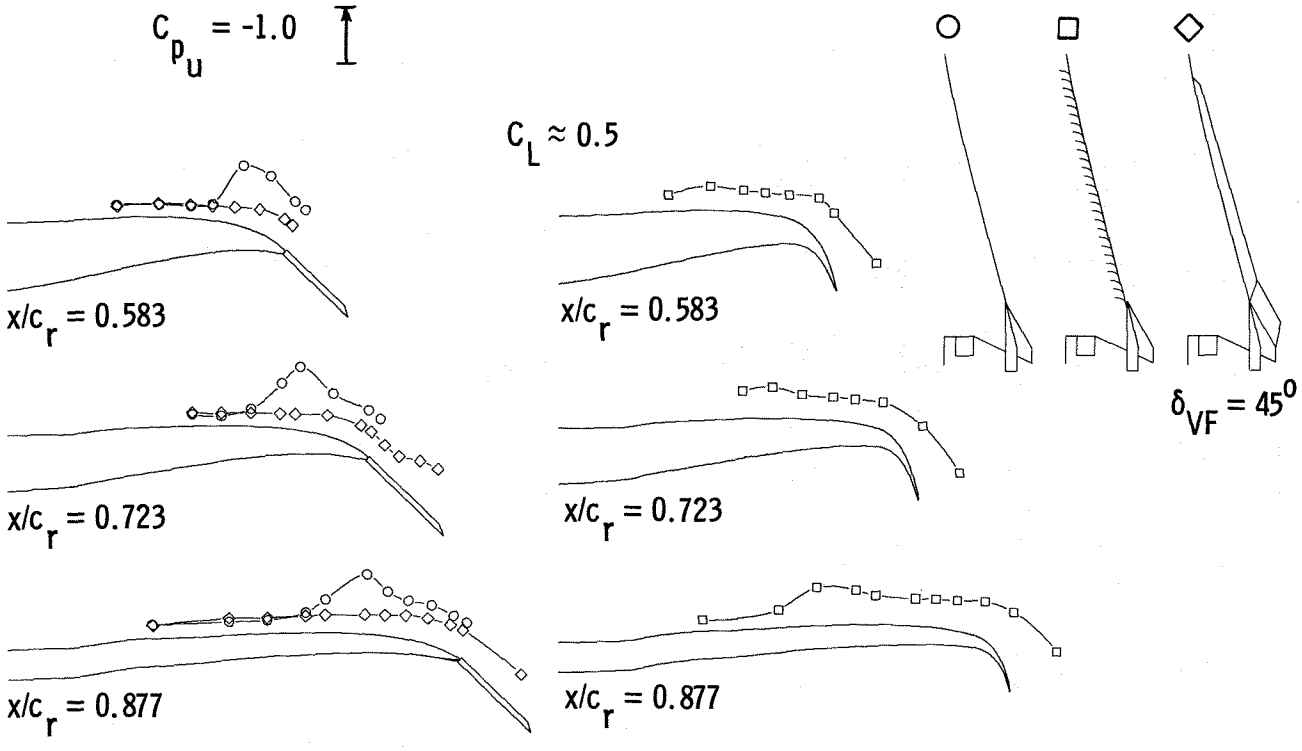

(a) $C_L \approx 0.5$

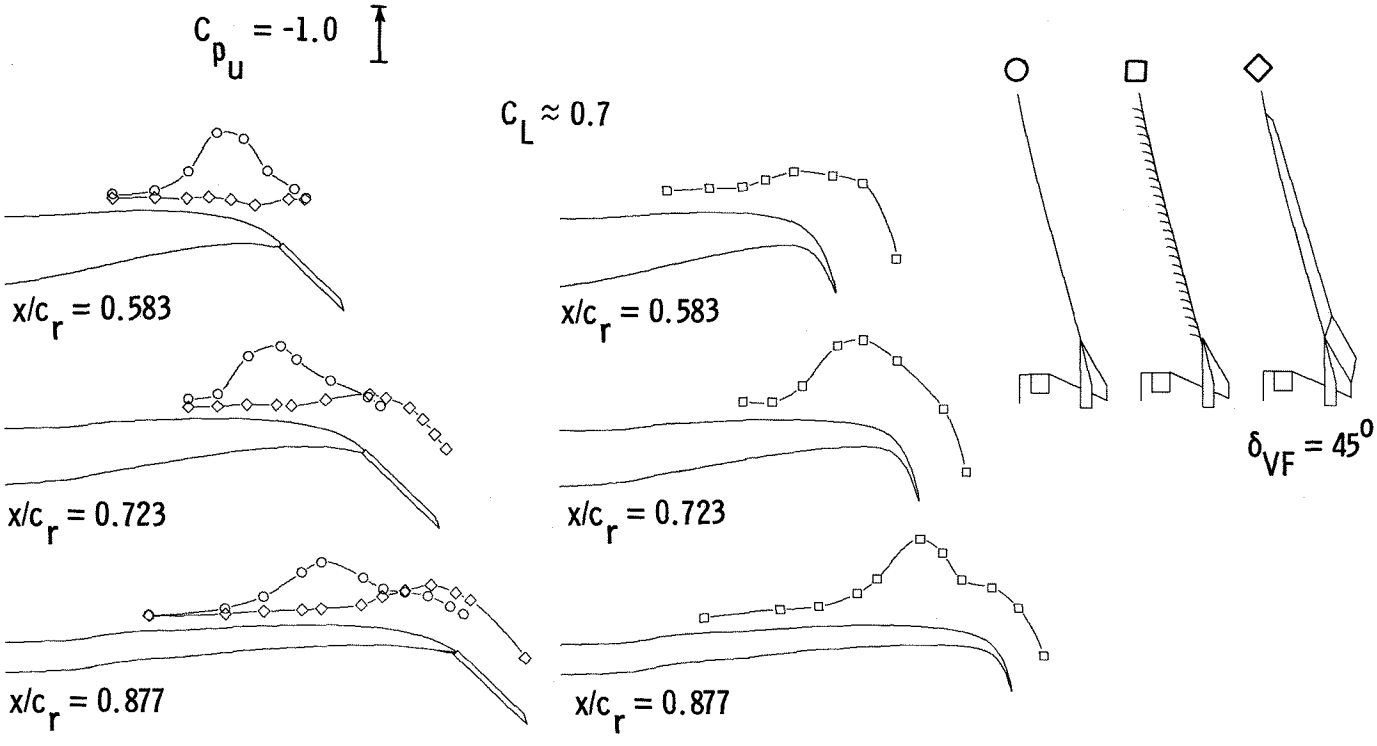

(b) $C_L \approx 0.7$

Figure 22. Cambered Leading-Edge/Vortex-Flap Comparison--Pitching Moment. $M_\infty = 0.3$, $\delta_{BF} = \delta_{EV} = 20^o$.

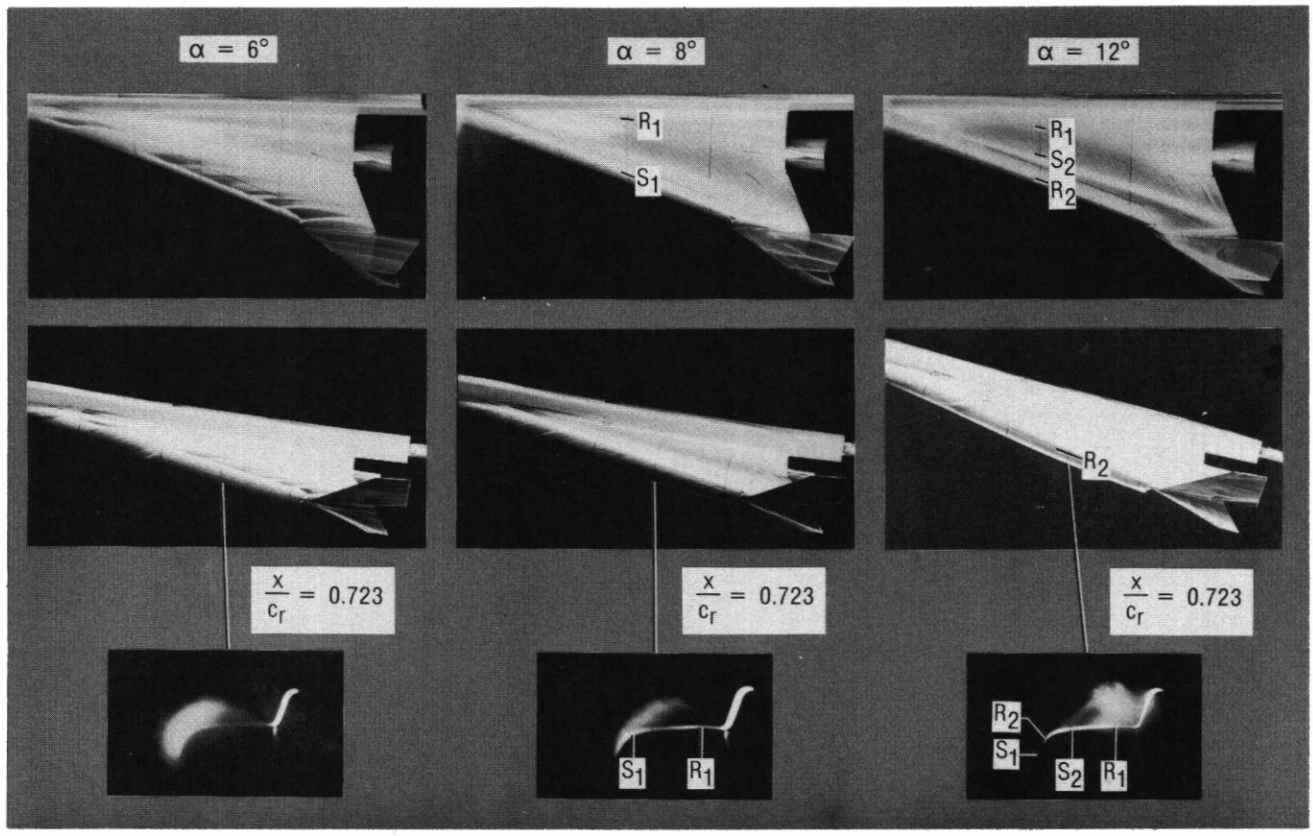

Figure 23. Cambered Leading-Edge Upper-Surface Streamlines and Cross-Flow Smoke Patterns. $\delta_{BF} = \delta_{EV} = 0^{o}$.

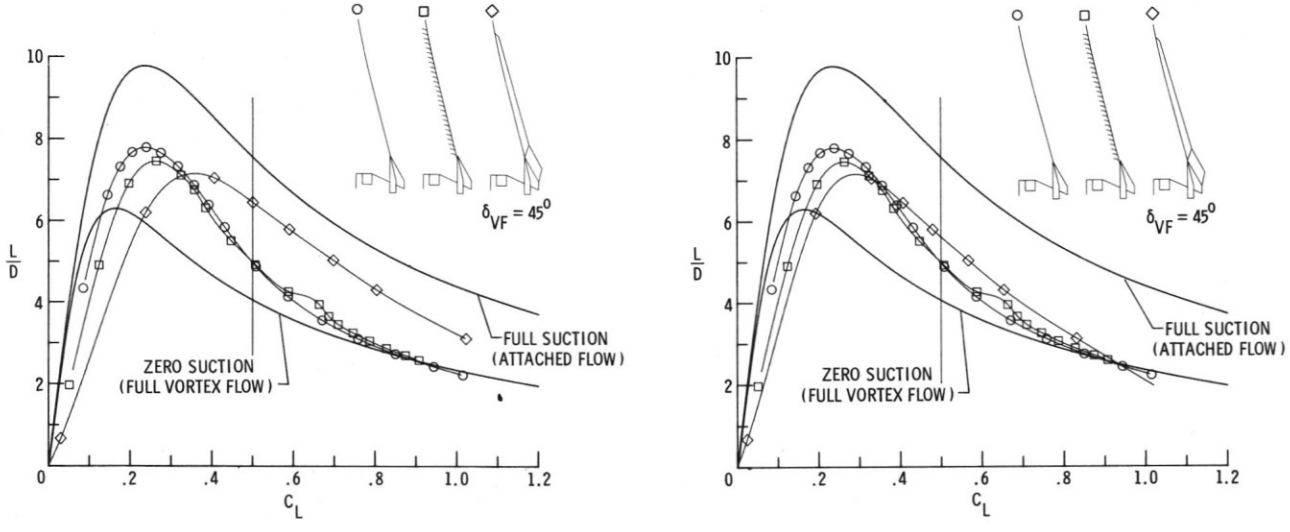

(a) Without Planform Area Correction

(b) With Planform Area Correction

Figure 24. Cambered Leading-Edge/Vortex Flap Comparison--Lift/Drag Ratio. $M_{\infty} = 0.3$, $\delta_{BF} = \delta_{EV} = 20^{o}$.